Tikrit Journal of Engineering Sciences (2023) 30 (4): 1-10

DOI: http://doi.org/10.25130/tjes.30.4.1

IRAQI Academic Scientific Journals

College of Engineering

ISSN: 1813-162X (Print); 2312-7589 (Online)

Tikrit Journal of Engineering Sciences

available online at: http://www.tj-es.com

TJES Tikrit Journal of Engineering Sciences

Performance Enhancement of LDPC Codes Based on Protograph Construction in 5G-NR Standard

Aymen M. Al-Kadhimi [a*], *A. E. Abdelkareem* [a], *Charalampos C. Tsimenidis* [b]

a College of Information Engineering/ Al-Nahrain University/ Baghdad/ Iraq.

b Department of Engineering/ Nottingham Trent University/ Nottingham/ UK.

Keywords:

Base Graph, Check/ Variable Nodes, Code Rate,LLR,.

ARTICLE INFO

Article history:

Received	01 Dec 2022
Received in revised form	25 June 2023
Accepted	03 July 2023
Final Proofreading	12 July 2023
Available online	01 Nov. 2023

Citation: Al-Kadhimi AM, Abdelkareem AE, Tsimenidis CC. Performance Enhancement of LDPC Codes Based on Protograph Construction in 5G-NR Standard *Tikrit Journal of Engineering Sciences* 2023; **30**(4): 1-10.

http://doi.org/10.25130/tjes.30.4.1

Corresponding author:

Aymen M. Al-Kadhimi

College of Information Engineering/ Al-Nahrain University/ Baghdad/ Iraq.

Abstract: To meet the high throughput demands, the 3rd Generation Partnership Project has specified the low-density parity check (LDPC) codes in the fifth generation-new radio 5G-NR standard with rate and length compatibility and scalability. This paper presents an extensive performance evaluation and enhancement of LPDC using the protograph-based construction defined in the 5G-NR standard. Firstly, the protograph-LDPC with layered offset min-sum (OMS) decoding, polar with successive cancellation list (SCL), and block turbo code are implemented and compared. Puncturing and shortening are applied to maintain block length at 1024 and code rate at 1/2 for all codes for comparison fairness. The results showed that P-LDPC outperforms its counterparts in terms of bit/ frame error rate (BER/ FER) behavior for given signal-to-noise ratios. Then, different P-LDPC settings were realized to study the effects of base graph selection (Graph1 or Graph2), code rate change (1/3 - 2/3), and block lengths increase (260 – 4160 bits). The simulation outcomes proved that BER performed better for lower coding rates or higher block lengths. Furthermore, P-LDPC behavior was examined over a Rayleigh flat-fading channel to achieve a 12.5 dB coding gain at 0.001 BER compared with uncoded transmission.

تحسين لأداء رموز فحص التماثل منخفض الكثافة تبعاً لهيكلية معيار شبكات الجيل الخامس

ايمن محمد حسن جعفر[1], عمار عبد الملك عبد الكريم[2], جارالمبوس تسيميندیس[3]
[1, 2] كلية هندسة المعلومات / جامعة النهرين / بغداد العراق.
[3] كلية العلوم والتكنلوجيا, قسم الهندسة, جامعة ترينت نوتنكهام, نوتنكهام, المملكة المتحدة

الخلاصة

لغرض تلبية متطلبات السرع العالية لشبكات اتصالات الجيل الخامس, قام مشروع شراكة الجيل الثالث بتعريف رموز فحص التماثل منخفض الكثافة مع سرع ترميز واطوال اكثر توافقية وقابلية للتوسع. تقوم هذه الورقة البحثية بتقييم وتحسين لأداء هذه الرموز بالاستفاده من طريقة هيكلة المصوفه تبعاً لمعيار شبكات الجيل الخامس. في البداية, تم مقارنة اداء رموز فحص التماثل منخفض الكثافة مع الرموز القطبية ورموز التوربين المهيكلة. بينت النتائج تفوق اداء رموز فحص التماثل منخفض الكثافة على قرائنها من حيث نسبة الخطأ. بعد ذلك, تم فحص هذه الرموز من حيث اختيار مخطط المصفوفه (رقم 1 او رقم 2), اختلاف معدل الترميز (3/1 – 2/1) و زيادة طول كتلة الرموز(260 – 4160). برهنت النتائج المستخلصة ان اداء معدل الاطارات الخاطئة يكون افضل كلما تم تقليل سرعة الترميز او زيادة طول كتلة البيانات. اضافة الى ما تقدم, قامت هذه الدراسة بفحص اداء هذه الرموز عند ارسالها عبر قناة مستوية التضاؤل لتبرهن اعطاء ربح في الترميز بما يعادل 12.5 ديسيبل مقارنة مع الارسال بدون ترميز.

الكلمات الدالة: الاقتطاع, رموز فحص التماثل منخفض الكثافة, عقد التأكيد/ التغيير, نسبة الترميز, هيكلة المصفوفه.

1.INTRODUCTION

One of the ultimate objectives of communication is to have a reliable connection. Forward error correction (FEC) techniques are implemented to improve data transmission reliability, which is achieved by adding extra redundant bits to the data (information) bits before being sent via a channel. Then, the coded bits can be uncoded on the receiver side to retrieve the original source bits. Consequently, the channel impairments are mitigated or even canceled due to applying well-designed codes [1]. According to Shannon's theory in 1948 [2], non-erroneous data transmission via noisy channels is achievable by appropriately designing FEC codes with a rate not exceeding the channel's capacity. Afterward, many FEC codes were investigated and developed, such as hamming code [3], LDPC codes [4], turbo codes [5], and polar code [6].

Particularly, the LDPC code has attracted researchers to investigate and develop them due to its capacity-approaching performance. However, one of the practical challenges of LDPC code is the high encoding complexity. To tackle this weakness, a structured LDPC class, called multi-edge type (MET) codes, has been presented [7]. P-LDPC codes have been proposed as a sub-class of MET codes offering low coding complexity and high error-resilience performance [8-12].

A protograph is a relatively minimized-number-of-nodes Tanner graph. Copying and permutation are the two main operations that derive larger sizes of a protograph construction. Whenever a protograph is copied M times, each edge of the protograph grows into a package of M edges that connect M check nodes (CNs) to M variable nodes (VNs). These replicas of the protograph are connected by performing permutation of the CN-to-VN pairs within every package. Consequently, the resultant code graph is M times larger than the code corresponding to the protograph with a similar rate and CN and VN distribution. Furthermore, by ensuring the permuting operation is circularly applied to every protograph edge, the derived code is adjustable to high decoding speeds. For example, Fig. 1 depicts a protograph with 3 VNs, 2 CNs, and five edges with the copy-and-permute operation.

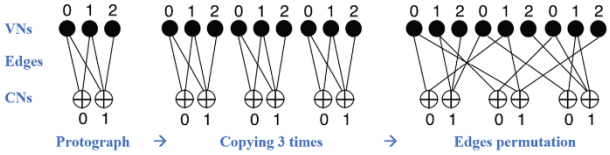

Fig. 1. Example of a Protograph Copying and Permutation.

The P-LDPC codes have attracted many research societies to adopt and develop these codes. The 3rd Generation Partnership Project (3GPP) is one of those communities that has deployed P-LDPC in practice as one of the main channel coding schemes in the 5G-NR standard [13]. This paper compares the performance of P-LDPC codes with other coding schemes and extensively evaluates different base graphs, code lengths, and code rates employed in the 5G-NR. This study considers the scenario of transmitting binary phase shift-keying (BPSK) symbols over additive white Gaussian noise (AWGN) and Rayleigh flat-fading channels.

In the past three decades, LDPC codes have been developed in literature by designers and researchers [14-16]. The channel coding has been the main scope of deployment of those LDPC codes for transmission over an AWGN channel [10, 17], a fading channel [18], and a relay-aided cooperative channel [19]. Hadamard-LDPC with a protograph structure

can be designed using Hadamard codes instead of single parity check (SPC) codes [20]. This designed code showed a capacity approaching 0.16 dB apart from the Shannon limit. On the other hand, LDPC and P-LDPC codes can be deployed as source coding schemes as in [21, 22], respectively. Nevertheless, LDPC can be concatenated with Luby-transform codes [23] to produce Raptor codes. These latter codes are applicable in transmitting video via wireless communication [24, 25], i.e., distributed source codes [26]. Moreover, LDPC and protograph-based LDPC codes can be implemented for both source and channel coding for multimedia communications [27, 28].

P-LDPC codes with rate compatibility have been investigated [29]. That compatibility can be utilized in adaptive-coding-based applications. In addition, LDPC with non-binary codes has been well analyzed and designed in [30, 31]. Those codes are seamlessly creating a combination with higher-order modulation schemes. Similarly, the non-binary codes were extended to the protograph structure design [32]. Other variants of protograph structure were developed for convolutional-based LDPC codes [33] and raptor-based codes [34]. In addition, to further minimize the realization complexity, quasi-cyclic P-LDPC codes were proposed by circular-permute regulations [35]. The P-LDPC codes have attracted many research societies to adopt and develop these codes. The 3rd Generation Partnership Project (3GPP) is one of those communities that has deployed P-LDPC in practice as one of the main channel coding schemes in the 5G-NR standard [13]. This paper compares the performance of P-LDPC codes with other coding schemes and extensively evaluates different base graphs, code lengths, and code rates employed in the 5G-NR. This study considers the scenario of transmitting binary phase shift-keying (BPSK) symbols over additive white Gaussian noise (AWGN) and Rayleigh flat-fading channels.

3.PROTOGRAPH CODE CONSTRUCTION

The LDPC code construction is mostly implemented in two stages: by optimizing a protograph that performs well in decoding; and by applying a progressive edge growth (PEG) algorithm [36]. This algorithm expands the chosen protograph for constructing the parity check matrix (H) with a minimized number of short cycles [37]. Otherwise, the resultant Tanner graph is unsatisfied with the protograph base constraints, and the high number of short cycles may cause performance degradation in the decoding phase [38].

In the 5G standard, one of two base graphs (BG) matrices (B_1 and B_2) is selected for constructing the LDPC H matrix. The matrices B_1 and B_2 are of sizes 46×68 and 42×52, respectively. The matrix H is obtained by replacing each element of B with a matrix with size $Z_c \times Z_c$, where Z_c is an expansion (or lifting) factor specified in the standard according to a set index i_{LS}, as shown in Table 1. The B's elements can be valued as $-1, 0, 1, \dots, Z_c - 1$, where each value is expanded as follows:

- Every entry of value -1 in B is replaced by an all-zero matrix of size $Z_c \times Z_c$;
- Each entry of value $i = 0, 1, \dots, Z_c - 1$ in B is replaced by identity matrix I of size $Z_c \times Z_c$ circularly shifted right i times.

For demonstration purposes, a mock example shows the paragraph construction for an LDPC code. Suppose a 3×6 base graph matrix B is defined in Eq. (1), and an expansion factor $Z_c = 5$ is selected. Each entity of B may have any integer value of -1 up to $Z_c - 1$. Each value of B is expanded into a 5×5 matrix, as shown in Eq. (2). For example, the value -1 is expanded into a 5×5 all-zero matrix, whereas 1 is expanded into a 5×5 identity matrix I circularly shifted right 1 time.

$$\mathrm{B} = \begin{bmatrix} 1 & -1 & 3 & 1 & 0 & -1 \\ 2 & 0 & -1 & 0 & 0 & 0 \\ -1 & 4 & 2 & 1 & -1 & 0 \end{bmatrix} \quad \textbf{(1)}$$

Table .1 P-LDPC Expansion Factor Sets [13]

Set index (i_{LS})	Set of expansion factor (Z_c)
0	{2, 4, 8, 16, 32, 64, 128, 256}
1	{3, 6, 12, 24, 48, 96, 192, 384}
2	{5, 10, 20, 40, 80, 160, 320}
3	{7, 14, 28, 56, 112, 224}
4	{9, 18, 36, 72, 144, 288}
5	{11, 22, 44, 88, 176, 352}
6	{13, 26, 52, 104, 208}
7	{15, 30, 60, 120, 240}

$$\mathrm{H} = \quad \textbf{(2)}$$

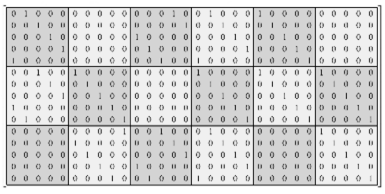

For LDPC in the 5G-NR standard, the base matrix B is constructed first in a protograph. Then, the matrix B is expanded to build the parity-check matrix H. The matrix B is structured in blocks defined below:

$$\mathrm{B} = \begin{bmatrix} A & E & O \\ B & C & I \end{bmatrix} \quad \textbf{(3)}$$

where the blocks' sizes are given below to build B_1 and B_2 with 46×68 and 42×52, respectively:
for $B_1 \rightarrow A: 4 \times 22, E: 4 \times 4, O: 4 \times 42$ all-zero; $B: 42 \times 22, C: 42 \times 4, I: 42 \times 42$ identity

for $B_2 \rightarrow A: 4 \times 10, E: 4 \times 4, O: 4 \times 38$ all-zero; $B: 38 \times 10, C: 38 \times 4, I: 38 \times 38$ identity

To further comprehend the construction process, an example of B_2 is shown in Fig. 2. According to Table 1; the selected parameters are $i_{LS} = 0$ and expansion factor $Z_c = 128$. The dots shown in the figure are drawn only for none -1 elements. In other words, those elements which expanded to zeros are ignored to visualize the non-zero effective elements better. The blocks A, E, B, C, and I are depicted in colors in Fig. 2. Each dot drawn in the figure will be expanded into 128. For instance, every blue dot appearing in the I block has a value of 0 in B_2 and will expand into a 128×128 identity matrix in H.

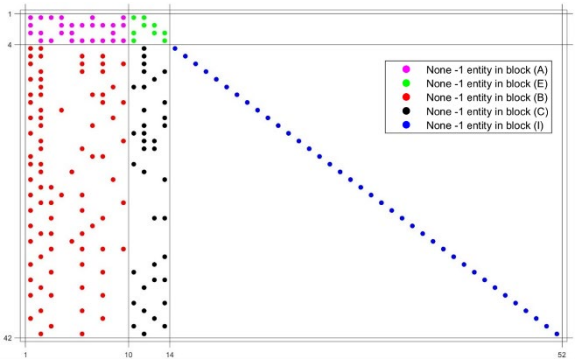

Fig. 2 Example of B_2 Matrix Drawn with Only None -1 Elements.

4.ENCODING IN THE 5G STANDARD

For the sake of simplicity, an example of a (4×8) B matrix is considered, as depicted in Eq. (4). Again, each element in B is expanded (lifted) by a factor of $Z_c = 5$.

$$B = \begin{bmatrix} 1 & -1 & 3 & 1 & 2 & 0 & -1 & -1 \\ 2 & 0 & -1 & 3 & -1 & 0 & 0 & -1 \\ -1 & 4 & 2 & 0 & 1 & -1 & 0 & 0 \\ 4 & 1 & 0 & -1 & 2 & -1 & -1 & 0 \end{bmatrix} \quad \textbf{(4)}$$

Equation (4) can be rewritten with another notation for a more appropriate mathematical representation shown afterward. The resultant graph matrix becomes as follows:

$$B = \begin{bmatrix} I_1 & 0 & I_3 & I_1 & I_2 & I & 0 & 0 \\ I_2 & I & 0 & I_3 & 0 & I & I & 0 \\ 0 & I_4 & I_2 & I & I_1 & 0 & I & I \\ I_4 & I_1 & I & 0 & I_2 & 0 & 0 & I \end{bmatrix} \quad \textbf{(5)}$$

where I_i is a 5×5 identity matrix circularly shifted right i times;

The B matrix in Eq. (5) has $(n-k) \times n$ dimension. Hence, in the systematic form:

- The message is represented as $M = [m_1\ m_2\ m_3\ m_4]$, where m_i is 5 bits.
- The codeword is represented as $C = [m_1\ m_2\ m_3\ m_4\ p_1\ p_2\ p_3\ p_4]$, where p_i is 5 bits parity-check part.

To perform encoding, the linear block codes' well-known formula is applied using Eq. (6) to reveal the four equations in Eq. (7) through Eq. (10).

$$BC^T = 0 \quad \textbf{(6)}$$

$$I_1 m_1 + I_3 m_3 + I_1 m_4 + I_2 p_1 + I p_2 = 0 \quad \textbf{(7)}$$

$$I_2 m_1 + I m_2 + I_3 m_4 + I p_2 + I p_3 = 0 \quad \textbf{(8)}$$

$$I_4 m_2 + I_2 m_3 + I m_4 + I_1 p_1 + I p_3 + I p_4 = 0 \quad \textbf{(9)}$$

$$I_4 m_1 + I_1 m_2 + I m_3 + I_2 p_1 + I p_4 = 0 \quad \textbf{(10)}$$

By adding the four preceding formulae, they yield:

$$I_1 p_1 = I_1 m_1 + I_3 m_3 + I_1 m_4 + I_2 m_1 + I m_2 + I_3 m_4 + I_4 m_2 + I_2 m_3 + I m_4 + I_4 m_1 + I_1 m_2 + I m_3 \quad \textbf{(11)}$$

Hence, the first parity-check p_1 is determined. Then, p_1 is substituted in Eq. (7) to find p_2. p_2 is substituted in Eq. (8) to find p_3, and p_1 and p_3 are substituted in Eq. (9) to find p_4.

The way the B matrix is structured is called double-diagonal. That structure, shown in blue in Eq. (5), is well designed to help the encoding phase in P-LDPC codes in the 5G standard.

After laying the ground in the preceding example, it is straightforward to understand the double-diagonal structure in B_1 and B_2 matrices in 5G. Again, B_2 with index $i_{LS} = 0$ and expansion factor $Z_c = 128$ is considered for demonstration, as appears in Eq. (12). The double-diagonal structure is surrounded and highlighted in blue color, which is block E in the structure in Eq. (3).

This B_2 matrix, shown in Eq. (12), has 42×52 dimension such that:

- The message is $[m_1\ m_2 \dots m_{10}]$, where m_i is 128 bits.
- The codeword is represented as $[m_1\ m_2 \dots m_{10}\ p_1\ p_2\ p_3\ p_4 \dots p_{42}]$, where p_i is 128 bits parity-check part.
- Using Eq. (6), the double-diagonal encoding uses the first four rows of B_2 to determine the parity checks $p_1, p_2, p_3, and\ p_4$.
- The 6th row is used to find p_6. The 7th row is used to find p_7, and so on through the last row to find p_{42}.

$B_2 =$

$$\begin{bmatrix} 9 & 117 & 76 & 26 & -1 & -1 & 61 & -1 & -1 & 77 & 0 & 0 & -1 & -1 & -1 & -1 & \cdots & \cdots & -1 & -1 \\ 39 & -1 & -1 & 38 & 125 & 125 & 98 & 28 & 96 & 124 & -1 & 0 & 0 & -1 & -1 & -1 & \cdots & \cdots & -1 & -1 \\ 81 & 114 & -1 & 44 & 52 & -1 & -1 & -1 & 112 & -1 & 1 & -1 & 0 & 0 & -1 & -1 & \cdots & \cdots & -1 & -1 \\ -1 & 8 & 58 & -1 & 30 & 104 & 81 & 54 & 18 & 0 & 0 & -1 & -1 & 0 & -1 & -1 & \cdots & \cdots & -1 & -1 \\ 51 & 86 & -1 & -1 & -1 & -1 & -1 & -1 & -1 & -1 & 71 & -1 & -1 & 0 & -1 & -1 & \cdots & \cdots & -1 & -1 \\ 103 & 41 & -1 & -1 & -1 & 66 & -1 & 31 & -1 & -1 & -1 & 103 & -1 & -1 & -1 & 0 & \cdots & \cdots & -1 & -1 \\ \vdots & \vdots & \vdots & \vdots & \vdots & \vdots & \vdots & \vdots & \vdots & \vdots & \vdots & \vdots & \vdots & \vdots & \vdots & \vdots & \ddots & \ddots & \vdots & \vdots \\ \vdots & \vdots & \vdots & \vdots & \vdots & \vdots & \vdots & \vdots & \vdots & \vdots & \vdots & \vdots & \vdots & \vdots & \vdots & \vdots & \ddots & \ddots & \vdots & \vdots \\ -1 & -1 & 0 & -1 & -1 & -1 & -1 & -1 & -1 & 75 & -1 & -1 & 120 & -1 & -1 & \cdots & \cdots & 0 & -1 \\ -1 & 1 & -1 & -1 & -1 & 101 & -1 & -1 & -1 & -1 & -1 & 118 & -1 & -1 & -1 & -1 & \cdots & \cdots & -1 & 0 \end{bmatrix} \quad \textbf{(12)}$$

5. DECODING OF P-LDPC

The decoding of LDPC codes is done in a soft-in-soft-output (SISO) iterative manner. Although the iterative decoding based on the sum-product (SP) algorithm can excellently perform, the high complexity is an effective

concern in the implementation stage. Min-sum (MS) algorithm [39] has been proposed to reduce complexity by utilizing approximation in check nodes (CN) updates of log-likelihood ratio (LLR) calculations. However, that complexity reduction is considered a trade-off with decoding performance. To compensate for the decoding performance degradation of the MS algorithm, the offset MS (OMS) algorithm [40] has been presented. That compensation is achieved by applying a correction factor (α) added to the CN's output LLR directly.

In this paper, the following notation and assumption are set. The codeword $C = \{c_1\ c_2\ \dots\ c_I\}$ is characterized by a $J \times I$ parity-check matrix of LDPC code that is mapped using the BPSK scheme to produce $S = \{s_1\ s_2\ \dots\ s_I\}$ symbols by $s_i = 1 - 2c_i, i \in [1, I]$. Afterward, the symbol vector passes throughout an AWGN channel to result in a received vector $r_i = s_i + g_i, i \in [1, I]$, where g_i is a random variable that is zero-mean independent Gaussian with variance σ^2. Then, the SISO decoding is done based on LLRs exchanged between VN and CN governed by the decoding algorithm described below. The VNs set involved in CN (cn_j) is determined as $M(j) = \{i \mid h_{i,j} = 1\}$. Correspondingly, the CNs set that participates in VN (vn_i) is denoted as $N(i)$. The two vectors L_{ij} and L_{ji} refer to LLR information being transmitted from variable-node vn_i to check-node cn_j or, on the contrary, from check-node cn_j to variable-node vn_i, respectively.

The OMS algorithm is summarized as follows:

1st step (Initialization): for $k = 0$ *and for every* $vn_i, i \in [1, I]$

$L_{ij}^0 = r_i$

2nd step (check-node computation): update $cn_j, j \in [1, J]$

$$L_{ji,MS}^k = \left(\prod_{i' \in M(j) \setminus i} sign\left(L_{i'j}^{k-1}\right) \right) \cdot \min_{i' \in M(j) \setminus i} \left| L_{i'j}^{k-1} \right|$$

$L_{ji}^k = max\{|L_{ji,MS}^k| - \alpha, 0\}$

3rd step (variable-node computation): the kth output of $vn_i, i \in [1, I]$

$$L_i^k = L_i^0 + \sum_{j \in N(i)} L_{ji}^k$$

$c_i^k = \left(1 - sign\left(L_i^k\right)\right)/2;\ X^k = C^k H^T$

if $X^k = 0$, *finish decoding and set the output* $\tilde{C} = C^k$

4th step: update $vn_i, i \in [1, I]$

$L_{ij}^k = L_i^k - L_{ji}^k, j \in N(i)$

increase k and go to 2nd step

The 5G NR standard supports layering in decoding to employ fewer iterations, leading to faster convergence. That is because the scheduling mechanism of this technique allows for the updated LLR messages on a layer to be utilized within the same iteration to perform new check-node calculations instead of waiting for all column and row calculations to produce new messages [41]. Layered decoders basically bundle the parity check matrix's rows into a certain number of groups; each is called a layer. An illustrative example is shown in Eq. (13), in which the H matrix rows are grouped to construct two layers. Suppose C_1 *and* C_2 are defined as the codes with H_1 *and* H_2 as parity check matrices, respectively. The layered decoding is shown in Fig. 3. The LLRs depicted in the figure refer to variable-node (matrix's columns) updates. The channel LLR is used by the decoder of C_1 in the first iteration; only then LLR_{21} is applied. That layering decoding would result in a reduction in the number of iterations for the decoder to converge.

In terms of B base graph matrices in 5G standard, each row block is treated as a layer for decoding. In other words, in the case of B_2, it is being processed as 42 layers since it has 42-row blocks.

$$H = \begin{bmatrix} H_1 \\ H_2 \end{bmatrix} = \begin{bmatrix} 1 & 1 & 1 & 0 & 1 & 0 & 0 \\ 0 & 0 & 0 & 1 & 0 & 1 & 1 \end{bmatrix} \} layer1 \\ \begin{bmatrix} 1 & 1 & 0 & 1 & 0 & 0 & 1 \\ 0 & 0 & 1 & 0 & 1 & 1 & 0 \end{bmatrix} \} layer2 \quad \textbf{(13)}$$

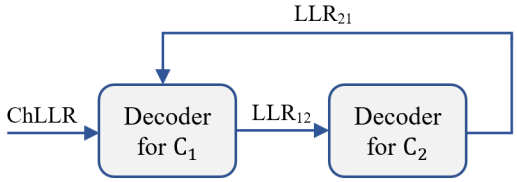

Fig. 3. Example of Layered Decoding Structure

6. PUNCTURING FOR RATE MATCHING

The method of eliminating some parity check bits from the codewords is called puncturing. This process increases the code rate, which in turn involves sending more information message bits. In the 5G NR standard, different code rates are achievable via puncturing parts of the base graph matrix. If the base graph 1 (i.e., B_1) is considered, the 46×68 base matrix will expand to $46Z_c \times 68Z_c$ parity check matrix H with $68Z_c - 46Z_c = 22Z_c$ message bits. The first two column message blocks of B_1, or equivalently first $2Z_c$ message bits, are punctured in 5G NR before transmission. Fig. 4 shows how puncturing of B_1 is employed to offer different code rates. If all remaining 66 blocks, or equivalently $66Z_c$ bits, are considered for transmission, the resultant code rate is $R = 22Z_c/66Z_c = 1/3$, as shown in blue color in Fig. 4.

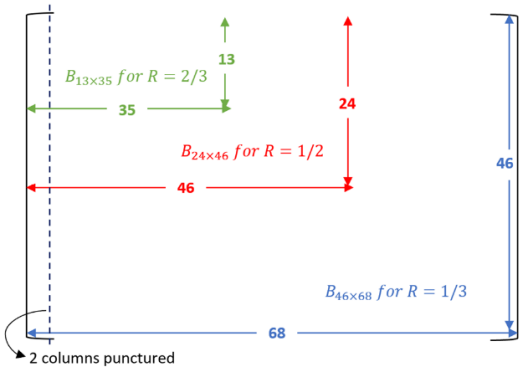

Fig. 4 Puncturing of B_1 Matrix for Several Different Rates

To increase the rate, some parts of the B_1, or equivalently H, are removed or punctured. In the case of transmitting the first $44Z_c$ bits, i.e., $20Z_c$ message bits $+24Z_c$ parity bits, and puncturing the last $22Z_c$ bits that result in $R = 22Z_c/44Z_c = 1/2$. That means only the 24×46 or $24Z_c \times 46Z_c$ upper-left part of B_1 or H, respectively, is used as appeared in red in the figure. To further increase the rate, only the first $33Z_c$ bits, i.e., $20Z_c$ message bits $+13Z_c$ parity bits, are sent to result in $R = 22Z_c/33Z_c = 2/3$. This rate is achieved by considering only the 13×35 upper-left part of B_1, as represented in green in the figure. Other variants of rates are allowed, and the same puncturing mechanism is correspondingly applicable for B_2. Bit interleaving is the second stage used in standard after puncturing for rate matching in higher-order modulation. However, this study considers only puncturing since the BPSK scheme is applied.

7. RESULTS

7.1. Results of P-LDPC vs. Other Coding Schemes

First, the P-LDPC code's performance is compared with polar codes [6] and block turbo codes [42]. For the P-LDPC code, base graph 2 (BG2), expansion factor $Z_c = 52$, and layered OMS decoding were chosen for evaluation purposes. For polar codes, the selected decoding algorithm is the successive cancellation list (SCL) [43] with list sizes (L=4 and L=8) aided by a cyclic redundancy check (CRC) with 11 bits long [13, 44]. For block turbo codes, a 2-dimension turbo product code (2-D TPC) is chosen by serially concatenating an extended Bose–Chaudhuri–Hocquenghem (BCH) code and an extended Hamming code. For all codes above, the codeword length was $n \approx 1024$, and puncturing/ shortening was performed to offer a code rate of $R = 1/2$ for comparison fairness. The number of transmitted blocks was kept at 50000 at its peak with a maximum number of iterations of 20. The scenario of transmitting coded BPSK symbols over an AWGN was assumed.

The frame (or block) error rate (FER) and bit error rate (BER) were calculated for different values of bit energy to noise spectral density ratio (E_b/N_0), as depicted in Fig. 5.

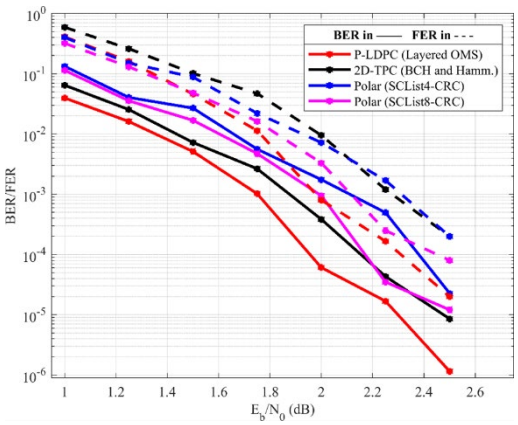

Fig. 5. Error Rates Performance for Different Schemes: $n \approx 1024, R = 1/2$

For BER, shown in solid lines, all codes' curves are growing progressively as the E_b/N_0 increases but with different rates of change. They show convergence in performance for low values of E_b/N_0 and start to diverge for higher dB values. The Polar SCList8-CRC offers better BER and FER behavior than Polar SClist4-CRC since the list size is double, which allows for better bit-wise decoding. On the other hand, 2D-TPC proposes a better BER than Polar codes for almost all dB values. Even though each of Polar SCList4-CRC, Polar SCList8-CRC, and 2D-TPC codes gave a reasonably good performance, it is explicitly shown that P-LDPC offers the best behavior in terms of both FER and BER compared with its counterparts.

7.2. Results of P-LDPC with Different Settings

After getting the P-LDPC evaluated and compared with other coding schemes, this section discusses some simulation results of P-LDPC with various selections of base graphs, block lengths, and coding rates. The layered OMS decoding and BPSK over AWGN were adopted.

For base graphs, according to Table 1, index $i_{LS} = 1$ with expansion factor $Z_c = 24$ and $i_{LS} = 6$ with $Z_c = 52$ were selected for BG1 and BG2, respectively. The two matrices, B_1 and B_2, were punctured to produce a code rate $R = 1/2$. After getting punctured, each row of BG1, i.e., in B_1, became 44 long and expanded to $44 \times 24 = 1056$ bits as codeword length (n). Similarly, BG2 produced $20 \times 52 = 1040$ bits as codeword length (n). Consequently, the two base graphs were expanded to those specific expansion factor values to guarantee each generates $n \approx 1024$ for comparison fairness. Fig. 6 shows that the two codes behave well with enhancement as E_b/N_0 increases. Both codes perform steadily,

almost similar for the region between $E_b/N_0 =$ 1 and 1.75 dB, with a small divergence above that value. In general, it is explicit that the code generated by BG2 outperforms that produced by BG1 in terms of FER and BER for higher E_b/N_0. That is because the recommended selection of base graphs, especially for $R = 1/2$, is BG2 [13].

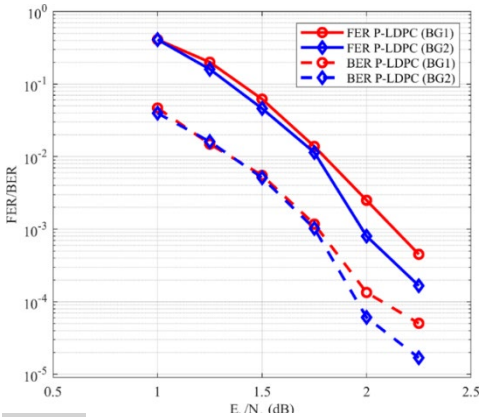

Fig. 6. Error Rates Performance of P-LDPC: $n \approx 1024,\ R = 1/2$.

As the number of iterations contributes to decoding complexity, it is beneficial to consider that in this context. Fig. 7 shows how many iterations the same two base graphs with $R = 1/2$ require to achieve a certain FER for different values of E_b/N_0. As depicted in Fig. 7, the number of iterations is inversely proportional to E_b/N_0. Even though BG1 requires two more iterations than BG2 at the launch of the graph, both codes converge and perform similarly for higher E_b/N_0 to achieve only four iterations for each code at $E_b/N_0 = 2.5$ dB.

To investigate the impact of increasing/ decreasing the block lengths on the code's performance, BG2 with $R = 1/2$ was applied with different values of expansion factors. All available factors at index $i_{LS} = 6$ were selected, i.e., $Z_c = 13, 26, 52, 104,$ and 208, which produce $n = 260, 520, 1040, 2080,$ and 4160 bits, respectively. In terms of BER

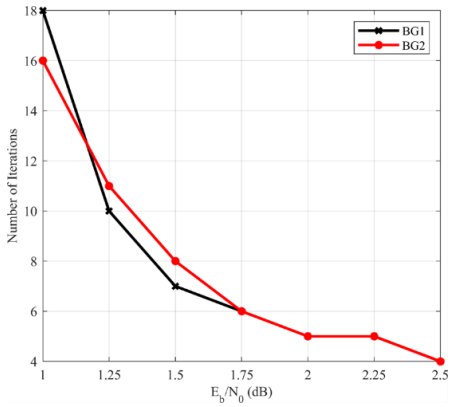

Fig. 7. Number of Iteration Performance: $n \approx 1024, R = 1/2$

performance, Fig. 8 exposes the poorest behavior, presented by the shortest length at $n = 260$. In contrast, the sharpest decline that indicates the best performance is noted at the longest length, $n = 4160$, to offer a BER of 0.00001 at 1.5 dB of E_b/N_0. For FER performance, Fig. 9 depicts the same behavior that explicitly shows that the codes' performance is excellently improved as their block lengths get longer. Nevertheless, the code complexity and block length are a matter of compromise.

The coding rate at all the preceding scenarios was fixed at $R = 1/2$. However, variants of the

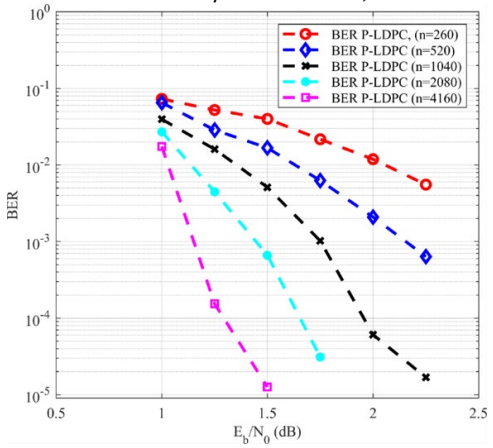

Fig. 8. BER Performance: $R = 1/2$ with Different Values Of n

rates are important to study. BG1 and BG2 construction allows for several coding rates via puncturing. BG2 was chosen to evaluate the performance at $R = 1/3, 2/5, 1/2,$ and 2/3. Fig. 10 shows the BER performance of those different coding rates in BG2. It is distinct that as the coding rate increased, the BER curve was shifted to the right for higher E_b/N_0. It indicates that the puncturing part of a codeword is beneficial for transmitting more information bits but at the expense of performance degradation. For the highest rate at $R = 2/3$, a 3.25 dB of E_b/N_0 is required to achieve a BER of 0.00003. This BER is effectively offered by the

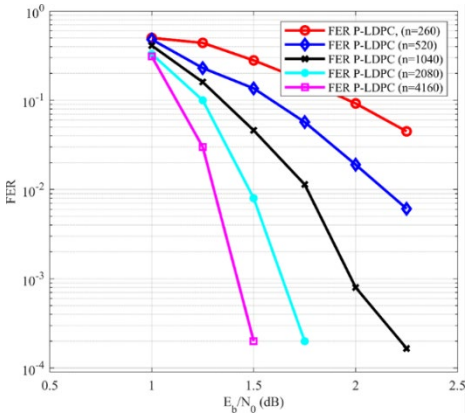

Fig. 9. FER Performance: $R = 1/2$ with Different Values of n

code with $R = 1/3$ and only 1.55 dB. In general, the less the coding rate, the sharper fall (better) the graph. Consequently, there is a compromise in terms of coding rate and performance for P-LDPC codes in the 5G NR standard and for other codes in general.

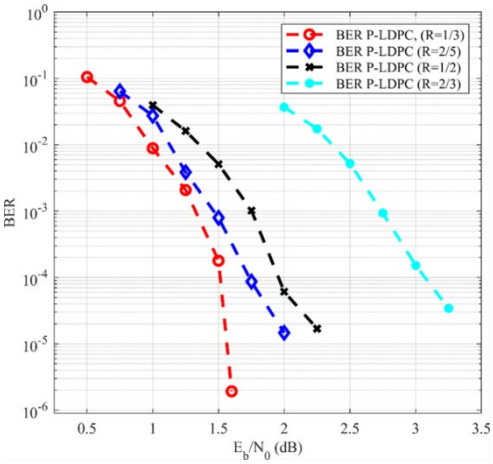

Fig. 10. BER Performance for Different Values of Rate R

7.3. Results of P-LDPC Over a Rayleigh Channel

Unlike the previous two sections, the P-LDPC evaluation was performed by transmitting data via a Rayleigh flat-fading channel instead of an AWGN channel. The block length and code rate were maintained at 1024 and 1/2, respectively. Fig. 11 depicts that the P-LDPC behavior is reasonably good since it offers a BER of 0.00003 at $E_b/N_0 = 11.5\ dB$. Moreover, it is shown that the uncoded BPSK requires 24 dB to achieve a BER of 0.001, while it takes only 11.5 dB for P-LDPC-coded BPSK to offer the same level of BER. Consequently, the P-LDPC code proposes a 12.5 dB coding gain.

Furthermore, the performance of P-LDPC will undoubtedly be improved for longer block lengths and/or lower coding rates.

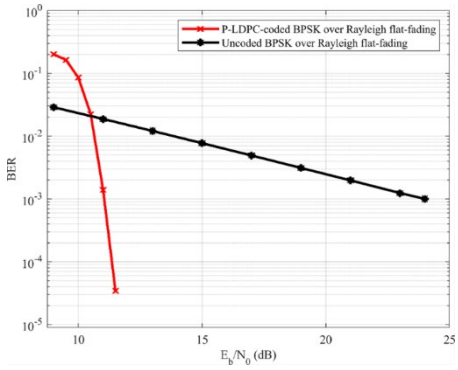

Fig. 11. P-LDPC Performance over a Rayleigh Flat-Sading Channel: $n \approx$

8. CONCLUSION

This study enhances the P-LDPC code performance based on base graph construction specified in the 5G-NR standard. The BER/FER behavior was evaluated using the OMS algorithm with layering for P-LDPC. The simulation results showed that this constructed code excellently behaved well as E_b/N_0 increased and outperformed its counterparts, such as CRC-aided polar SCL and TPC. The variant expansion factors were adopted to achieve different codeword lengths, and puncturing was exploited to raise the code rate from 1/3 through 2/3. Based on the results, it is explicit how an increase in coding rate and a decrease in code word length would lead to performance degradation. Furthermore, P-LDPC performed well when coded-BPSK symbols transmitted over a Rayleigh flat-fading channel to deliver 12.5 dB coding gain at 0.001 BER compared with the uncoded transmission.

On the other hand, the presented P-LDPC code can be further enhanced for future work. Firstly, more efficient mechanisms of the extrinsic LLR exchange among CNs and VCs can be adopted to improve code performance. Secondly, the OMS algorithm might be implemented with an early stopping criterion. That means the decoding process would end once a certain threshold of message beliefs is achieved. Consequently, instead of running 20 iterations (used in this paper), an approach similar to BER will be offered by fewer iterations. Thirdly, the implemented code performance in this study is bad over the frequency-selective channel. Hence, further consideration of the high Doppler effect might be examined. The system can perform better by realizing an equalizer over MIMO-OFDM channels [45]. Fourthly, higher-order modulation schemes, such as 16-QAM and 64-QAM, can be investigated to examine the code's behavior [46], especially with CRC attachment. Lastly, this study is initially intended to be applied over an AWGN channel, and then, it will be extended to realize P-LDPC in the Internet of underwater things (IoUT). Underwater channels are very harsh environments where the Doppler shift is extremely high, and special adaptive compensation algorithms are crucial to implement to deal with such severe conditions [47].

REFERENCES

[1] Costello DJ, Forney GD. **Channel Coding: The Road to Channel Capacity**. *Proceedings of the IEEE* 2007; **95** (6): 1150-77.

[2] Shannon CE. **A Mathematical Theory of Communication**. *The Bell System Technical Journal* 1948; **27** (3): 379-423.

[3] Hamming RW. **Error Detecting and Error Correcting Codes**. *The Bell System Technical Journal* 1950; **29** (2): 147-60.

[4] Gallager RG. **Low-Density Parity Check Codes.** Cambridge: Massachusttes; 1963.

[5] Berrou C, Glavieux A, Thitimajshima P. **Near Shannon Limit Error-Correcting Coding and Decoding**: Turbo-codes.1. *ICC'93-IEEE International Conference on Communications 1993 May 23-26;* Geneva, Switzerland. IEEE: p. 1064-1070.

[6] Arikan E. **Channel Polarization: A Method for Constructing Capacity-Achieving Codes for Symmetric Binary-Input Memoryless Channels**. *IEEE Transactions on Information Theory* 2009; **55** (7): 3051-3073.

[7] Richardson T, Urbanke R. **Multi-Edge Type LDPC Codes**. *Workshop honoring Prof. Bob McEliece on his 60th birthday 2002 May 24;* California, USA. California Institute of Technology: p. 24-25.

[8] Thorpe J. **Low-Density Parity-Check (LDPC) Codes Constructed from Protographs.** *IPN Progress Report*; 2003; 42 (154): pp. 42-154.

[9] Divsalar D, Jones C, Dolinar S, Thorpe J. **Protograph Based LDPC Codes with Minimum Distance Linearly Growing with Block Size**. *Global Telecommunications Conference GLOBECOM* 2005 Nov 28-Dec 2; St. Louis, MO, USA. IEEE: p. 1152-1156.

[10] Divsalar D, Dolinar S, Jones CR, Andrews K. **Capacity-approaching Protograph Codes**. *IEEE Journal on Selected Areas in Communications* 2009; **27** (6): 876-888.

[11] Abu-Surra S, Divsalar D, Ryan WE. **On The Existence of Typical Minimum Distance for Protograph-Based LDPC Codes**. *Information Theory and Applications Workshop (ITA)* 2010 Jan **31**(5); La Jolla, CA, USA. IEEE: p. 1-7.

[12] Abu-Surra S, Divsalar D, Ryan WE. **Enumerators for Protograph-based Ensembles of LDPC and Generalized LDPC Codes**. *IEEE Transactions on Information Theory* 2011; **57** (2): 858-886.

[13] Access, E. U. T. R. (2010). **Multiplexing and channel coding**," 3rd Generation Partnership Project (3GPP). *TS*, 36, v10.

[14] MacKay DJ, Neal RM. **Good Codes Based on Very Sparse Matrices**. *IMA* International Conference on Cryptography and Coding 1995 Dec; Berlin, Heidelberg. Springer: p. 100-111.

[15] Richardson TJ, Urbanke RL. **The Capacity of Low-Density Parity-Check Codes under Message-Passing Decoding**. *IEEE Transactions on information theory* 2001; **47** (2): 599-618.

[16] Fang Y, Bi G, Guan YL, Lau FC. **A Survey on Protograph LDPC Codes and their Applications**. *IEEE Communications Surveys & Tutorials* 2015; **17** (4): 1989-2016.

[17] Yang Z, Fang Y, Zhang G, Lau FC, Mumtaz S, Da Costa DB. **Analysis and Optimization of Tail-Biting Spatially Coupled Protograph LDPC Codes for BICM-ID Systems**. *IEEE Transactions on Vehicular Technology*. 2019; **69** (1): 390-404.

[18] Fang Y, Chen P, Cai G, Lau FC, Liew SC, Han G. **Outage-limit-Approaching Channel Coding for Future Wireless Communications: Root-Protograph Low-density Parity-Check Codes**. *IEEE Vehicular Technology Magazine*. 2019; **14** (2): 85-93.

[19] Fang Y, Liew SC, Wang T. **Design of Distributed Protograph LDPC Codes for Multi-relay Coded-cooperative Networks**. *IEEE Transactions on Wireless Communications*. 2017; **16** (11): 7235-51.

[20] Zhang PW, Lau FC, Sham CW. **Protograph-based LDPC Hadamard Codes**. *IEEE Transactions on Communications* 2021; **69** (8): 4998-5013.

[21] Liveris AD, Xiong Z, Georghiades CN. **Compression of Binary Sources with Side Information at the Decoder Using LDPC Codes**. *IEEE Communications Letters* 2002; **6** (10): 440-442.

[22] Ye F, Dupraz E, Mheich Z, Amis K. **Optimized Rate-Adaptive Protograph-Based LDPC Codes for Source Coding with Side Information**. *IEEE Transactions on Communications* 2019; **67** (6): 3879-89.

[23] Luby M. **LT Codes**. *43rd* Annual IEEE Symposium on Foundations of Computer Science 2002 Nov 19; Vancouver, BC, Canada. IEEE Computer Society: p. 271-280.

[24] Wu J, Yuen C, Wang M, Chen J, Chen CW. **TCP-oriented Raptor Coding for High-Frame-Rate Video Transmission over Wireless Networks**. *IEEE Journal on Selected Areas in Communications* 2016; **34** (8): 2231-46.

[25] Wu J, Cheng B, Wang M. **Improving Multipath Video Transmission with Raptor Codes in Heterogeneous Wireless Networks**. IEEE Transactions on Multimedia 2017; **20** (2): 457-472.

[26] Fresia M, Vandendorpe L, Poor HV. **Distributed Source Coding Using Raptor Codes for Hidden Markov Sources**. *IEEE Transactions on Signal Processing* 2009; **57** (7): 2868-2875.

[27] Hanzo L. **Near-Capacity H. 264 Multimedia Communications Using Iterative Joint Source-Channel**

Decoding. *IEEE Communications Surveys & Tutorials* 2011; **14** (2): 538-564.

[28] Bi C, Liang J. **Joint Source-Channel Coding of Jpeg 2000 Image Transmission over Two-Way Multi-Relay Networks**. *IEEE Transactions on Image Processing* 2017; **26** (7): 3594-3608.

[29] Van Nguyen T, Nosratinia A. **Rate-Compatible Short-Length Protograph LDPC Codes**. *IEEE Communications Letters* 2013; **17** (5): 948-951.

[30] Dupraz E, Savin V, Kieffer M. **Density Evolution for the Design of Non-Binary Low Density Parity Check Codes for Slepian-Wolf Coding**. *IEEE Transactions on Communications* 2014; **63** (1): 25-36.

[31] Han G, Guan YL, Huang X. **Check Node Reliability-Based Scheduling for BP Decoding of Non-Binary LDPC Codes**. *IEEE Transactions On Communications* 2013; **61** (3): 877-885.

[32] Dolecek L, Divsalar D, Sun Y, Amiri B. **Non-Binary Protograph-Based LDPC Codes: Enumerators, Analysis, and Designs**. *IEEE Transactions On Information Theory* 2014; **60** (7): 3913-3941.

[33] Mitchell DG, Pusane AE, Costello DJ. **Minimum Distance and Trapping Set Analysis of Protograph-Based LDPC Convolutional Codes**. *IEEE transactions on information theory* 2012; **59** (1): 254-281.

[34] Wei L, Costello DJ, Fuja TE. **Coded Cooperation Using Rate-Compatible Spatially-coupled Codes**. *IEEE International Symposium on Information Theory* 2013 Jul 7-12; Istanbul, Turkey. IEEE: p. 1869-1873.

[35] Karimi M, Banihashemi AH. **On the Girth of Quasi-Cyclic Protograph LDPC Codes**. *IEEE Transactions On Information Theory* 2013; **59** (7): 4542-4552.

[36] Hu XY, Eleftheriou E, Arnold DM. **Regular and Irregular Progressive Edge-Growth Tanner Graphs**. *IEEE Transactions On Information Theory* 2005; **51** (1): 386-398.

[37] Healy CT, de Lamare RC. **Design of LDPC Codes Based on Multipath EMD Strategies for Progressive Edge Growth**. *IEEE Transactions on Communications* 2016; **64** (8): 3208-3219.

[38] Ye F, Dupraz E, Mheich Z, Amis K. **Optimized Rate-Adaptive Protograph-Based LDPC Codes for Source Coding with Side Information**. *IEEE Transactions on Communications* 2019; **67** (6): 3879-3889.

[39] Fossorier MP, Mihaljevic M, Imai H. **Reduced Complexity Iterative Decoding of Low-Density Parity Check Codes Based on Belief Propagation**. *IEEE Transactions on Communications* 1999; **47** (5): 673-680.

[40] Chen J, Fossorier MP. **Near Optimum Universal Belief Propagation-Based Decoding of Low-Density Parity Check Codes**. *IEEE Transactions on Communications* 2002; **50** (3): 406-414.

[41] Zhou Z, Peng K, Krylov A, Rashich A, Tkachenko D, Li F, Zhang C, Song J. **Enhanced Adaptive Normalized Min-Sum Algorithm for Layered Scheduling of 5G-NR LDPC Codes**. *International Symposium on Broadband Multimedia Systems and Broadcasting (BMSB)* 2020 Oct 27-29; Paris, France. IEEE: p. 1-5.

[42] Pyndiah RM. **Near-Optimum Decoding of Product Codes: Block Turbo Codes**. *IEEE Transactions on Communications* 1998; **46** (8): 1003–1010.

[43] Tal I, Vardy A. **List Decoding of Polar Codes**. *IEEE Transactions on Information Theory* 2015; **61** (5): 2213-2226.

[44] Niu K, Chen K. **CRC-Aided Decoding of Polar Codes**. *IEEE Communications Letters* 2012; **16** (10): 1668-1671.

[45] Shahab MM, Hardan SM, Hammoodi AS. **A New Transmission and Reception Algorithms for Improving the Performance of SISO/MIMO- OFDM Wireless Communication System**. *Tikrit Journal of Engineering Sciences* 2021; **28** (3): 146–158.

[46] Kuti AY, Abdelkareem AE. **Evaluation of Low-Density Parity-Check Code with 16-QAM OFDM in a Time-Varying Channel**. *International Conference on Communication, Networks and Satellite (COMNETSAT)* 2021 July 17-18; Purwokerto, Indonesia. IEEE: p. 128-134.

[47] Abdelkareem AE, Sharif BS, Tsimenidis CC. **Adaptive Time Varying Doppler Shift Compensation Algorithm for OFDM-Based Underwater Acoustic Communication Systems**. *Ad Hoc Networks* 2016; **45**: 104-119.